Remote Sensing Applications: Society and Environment 32 (2023) 101050

Contents lists available at ScienceDirect

Remote Sensing Applications: Society and Environment

journal homepage: www.elsevier.com/locate/rsase

Developing a satellite-based combined land degradation index for monitoring environmental change: A case study in Tana-Beles watershed, Upper Blue Nile, Ethiopia

Abeyou W. Worqlul [a, *], Mira Haddad [b], Sintayehu Alemayehu [c], Ajit Govind [d]

[a] International Center for Agricultural Research in the Dry Areas (ICARDA), Addis Ababa, Ethiopia
[b] International Center for Agricultural Research in the Dry Areas (ICARDA), Amman, Jordan
[c] International Center for Tropical Agriculture (CIAT), Nairobi, Kenya
[d] International Center for Agricultural Research in the Dry Areas (ICARDA), Cairo, Egypt

ARTICLE INFO

Keywords:
Albedo
Soil salinity
Landsat
Vegetation condition

ABSTRACT

Land degradation is one of the most pressing environmental challenges due to its effect on the people and ecosystem. Early detection of land degradation could help to avoid further deterioration and work on reversing the trend. This would require an integrated approach combining indicators such as vegetation condition, soil health (i.e., soil salinity), and soil exposure (i.e., albedo) to characterize land degradation comprehensively. Therefore, this study aims at developing a satellite image-based combined land degradation index to monitor the spatial extent of land degradation in the Upper Blue Nile Basin, Ethiopia. In addition, the study also evaluates the environmental change associated with land degradation across the Tana-Beles watershed. The combined land degradation index (CLDI) was developed by integrating multiple indicators, including normalized vegetation Index (NDVI), salinity index (SI), and albedo, for two periods spanning between 1990 and 2000 (1990s) and 2010 to 2020 (2010s). The individual indicators were combined with Principal Component Analysis (PCA) by assigning weights to the individual indicators. The analysis indicated that, in the 2010s, the vegetation condition deteriorated over 98.5% of the study area, while soil salinity and albedo increased by 82% and 97% in the 1990s, respectively. The combined land degradation index developed with the PCA indicated in the 2020s a fraction of the study area ~2% is extremely degraded, while 18%, 43%, 27%, and 10% of the site is strongly, moderately, slightly, and not degraded, respectively. Monitoring land degradation is important for countries like Ethiopia, where most of the county are occupied by semi-arid and arid climate zones.

1. Introduction

Land degradation has become an important global issue since the 21st century due to its adverse effect on people and ecosystems (Chen and Rao, 2008; Gibbs and Salmon, 2015). According to IPCC (Intergovernmental Panel on Climate Change), land degradation is defined as a negative trend in land conditions caused by direct or indirect human-induced processes, expressed as long-term reduction or loss of at least biological productivity, ecological integrity, or value to humans (Olsson et al., 2019). Land degradation has been worsening in many regions of the world, affecting the well-being of over two-fifths of humanity (Ferrer-i-Carbonell & Gowdy,

* Corresponding author.
E-mail address: a.worqlul@cgiar.org (A.W. Worqlul).

https://doi.org/10.1016/j.rsase.2023.101050
Received 17 March 2023; Received in revised form 4 August 2023; Accepted 22 August 2023
Available online 26 August 2023

2007; Haberl et al., 2007; Le et al., 2016). In fact, the situation of land degradation is worse in developing countries. In 1994, the UNCCD (United Nations Convention to Combat Desertification), ratified by 195 countries, has identified land degradation and desertification as one of our time's most pressing environmental issues (Olsson et al., 2019; UNCCD, 2002). The UNDC acknowledges that land degradation can be a result of various factors, including climate variability and human activity.

There are multiple indicators of land degradation; among them, vegetation condition, soil salinity, and soil exposure are widely used as a proxy for land degradation (Eckert et al., 2015; Ibrahim et al., 2015; Liu et al., 2017; Mariano et al., 2018; Wessels et al., 2004). In recent years, the availability of earth observation data helped to map land degradation, which was vital to understand the impacts of land degradation on social-ecological systems at various scales.

Multiple land degradation indicators have been developed to monitor land degradation (Chikhaoui et al., 2005; Higginbottom and Symeonakis, 2014). Most of the approaches used proxies to represent land degradation, for example, the Normalized Vegetation Index (NDVI) (Bai et al., 2008a; Easdale et al., 2018), salinity index (Manandhar and Odeh, 2014), and albedo (Liu et al., 2017; Yu et al., 2021). However, an integrated approach that combines multiple indicators such as vegetation condition, soil health (i.e., soil salinity), and soil exposure (i.e., albedo) to characterize land degradation is still lacking. A combined approach could provide better information to take appropriate policy making and intervention. For example, Analytic Hierarchy Process (AHP) and Principal Component Analysis (PCA) (Hoang et al., 2018) are the two popular holistic approaches to estimate land degradation. AHP is a qualitative and subjective approach, while PCA is an objective approach (Kong et al., 2018). The AHP method is used mainly to combine independent factors to evaluate land suitability for irrigation, crop production, groundwater recharge, etc. (Elaalem et al., 2011; Mallick and Rudra, 2021; Worqlul et al., 2022). The PCA approach has been applied to combine multiple indicators to develop combined drought monitoring indexes. Bayissa et al. (2019) used PCA to develop a combined drought monitoring index by combining four satellite-based input parameters (standardized precipitation index, normalized difference vegetation index, land surface temperature anomaly, and soil moisture anomaly).

Land degradation is a major environmental problem in Ethiopia. Gebreselassie et al. (2016) indicated that more than 85% of the country is moderately to severely degraded. Major drivers for Ethiopia's severe land degradation include soil erosion, rapid population growth, deforestation, and improper land and soil management (Taddese, 2001; Temesgen et al., 2014). Estimating land degradation and its impact is essential to implement appropriate remedial measures, improving environmental vitality, and building resilience. This study, therefore, aims to develop a comprehensive combined land degradation index (CLDI) in the Tana-Beles watershed of Ethiopia. The study also evaluated the impact of land degradation across the study site by evaluating land use change, and change in the river mouth delta of the major tributaries of Lake Tana. Lake Tana and Beles watersheds are the sub-watersheds of the upper Blue Nile Basin. Lake Tana and Beles watersheds were connected in May 2010 with a tunnel to generate hydropower via an inter-basin water transfer scheme. The Tana-Beles watershed provides a wide range of ecosystem services, and Lake Tana is the largest freshwater source in Ethiopia. The study area is considered as one of Ethiopia's growth corridors, where large-scale development projects such as the Grand Ethiopian Renaissance Dam (GERD) and the Tana-Beles sugar factory are underway. In Tana-Bele, soil erosion is one of the major problems in which the water quality of Lake Tana has been deteriorating significantly due to nutrient and sediment influxes creating a favorable environment for invasive aquatic crops (Dersseh et al., 2019; Worqlul et al., 2020).

2. Materials and methods

2.1. Study area

The study was carried out in the Tana-Beles watershed, Upper Blue Nile Basin of Ethiopia. Lake Tana and Beles watersheds have been connected through a tunnel since May 2010 for inter-basin water transfer to generate hydropower. The Tana-Beles watershed has a catchment area of 29,260 km^2, accounting for ~14.6% of the Upper Blue Nile Basin. Lake Tana is Ethiopia's largest lake, located within the Tana-Beles basin. The waterbody covers ~3060 km^2 at an altitude of 1786 m amsl (above mean sea level) extracted from a Shuttle Radar Topography Mission Digital Elevation Model (SRTM-DEM) (Farr et al., 2007). The Tana-Beles watershed extends between 10°22′N, 35°3′E and 12°50′N, 38°21′E (Fig. 1). The watershed has a complex topography with significant elevation variations ranging from 513 to 4094 m amsl. The highest point within the study area is situated on Mount Guna. The land use of the Lake Tana watershed is primarily agricultural land (Kebede et al., 2021), whereas the Beles watershed is predominantly covered by bushland and woodland (Surur, 2010).

2.1.1. Data availability and image preprocessing

The study relied on satellite-based remote sensing data to develop a CLDI. Landsat TM/ETM + and OLI data from 1990 to 2000 (hereafter called the 1990s) and 2010 to 2020 (hereafter called the 2010s) were used to estimate multiple land degradation indexes and land use change. The study used multiple Landsat images of paths 169,170, and 171 and rows 51, 52, and 53 (Fig. 2). For the 1990s, there were 1255 Landsat images within the study site, and for the 2010s, there were 1284 images available to estimate the individual land degradation indicators. Rainfall data, which was used to evaluate rainfall variability across the study site, was obtained from Climate Hazards Group InfraRed Precipitation with Stations (CHIRPS) (Funk et al., 2015). Table 1 presents the satellite data used for this study, including their spatial and temporal resolution. The satellite data acquisition and processing were conducted using the Google Earth Engine (GEE) cloud computation platform (Gorelick et al., 2017; Moore and Hansen, 2011). The data collected comprises Landsat TM/ETM + and OLI data at Level-2, representing atmospherically corrected surface reflectance. Level-2 data is derived from Collection 2 of Level-1 data, meeting the criteria of less than 76° Solar Zenith Angle and undergoing radiometric correction.

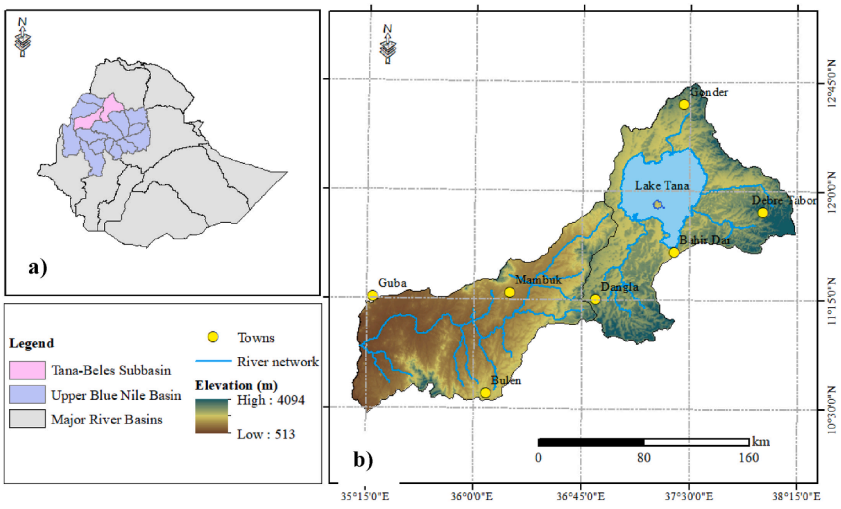

Fig. 1. Location of Tana-Beles watershed within the upper Blue Nile Basin of Ethiopia. (A) Ethiopia's major river basins and Tana-Beles watershed within the Upper Blue Nile Basin. (B) River network of the Tana-Beles watershed, a 30 m digital elevation model as a background. (For interpretation of the references to colour in this figure legend, the reader is referred to the Web version of this article.)

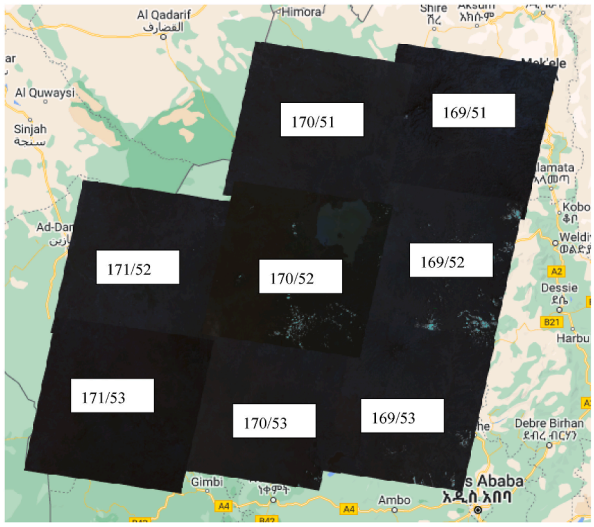

Fig. 2. Path and row of the Landsat images were used to develop a combined land degradation index of the Lake Tana-Bles basin from 1990 to 2000 (1990s) and 2000 to 2010 (2010s).

Table 1
The satellite data used to develop a combined land degradation index for the Tana-Beles watershed, including their spatial and temporal resolution.

Satellite	Period	Spatial resolution (m)	Temporal resolution (day)
Landsat 5/8	2010 to 2020	30	16
Landsat 5 TM	1990 to 2010	30	16
CHIRPS	1990 to 2020	5500	1

2.1.2. Climate variability of the tana-Beles watershed

The Tana-Beles watershed experiences a monomodal rainfall pattern. The main rainfall season (also called "*Kremt*") extends from June to September and accounts for up to 85% of the annual rainfall (Fig. 3). The dry season lasts from October to May with limited rainfall. The average annual rainfall from 1990 to 2020 varies between 890 and 2000 mm. The 30-year watershed averaged annual rainfall analysis indicated an increasing rainfall trend. High daily temperatures characterize the dry season.

The annual rainfall variability from 1990 to 2020 was evaluated with the rainfall anomaly index (RAI). It represents the number of standard deviations of the annual rainfall by which the observed rainfall deviates from the long-term average annual rainfall (Katz and Glantz, 1986; Worqlul et al., 2019). The rainfall analysis for the period 1990 to 2020 indicated that 3.2% of the time, the watershed had extremely wet and dry conditions, each with RAI >2 and RAI <-2, respectively (Table 2). While 16.1% of the time, the

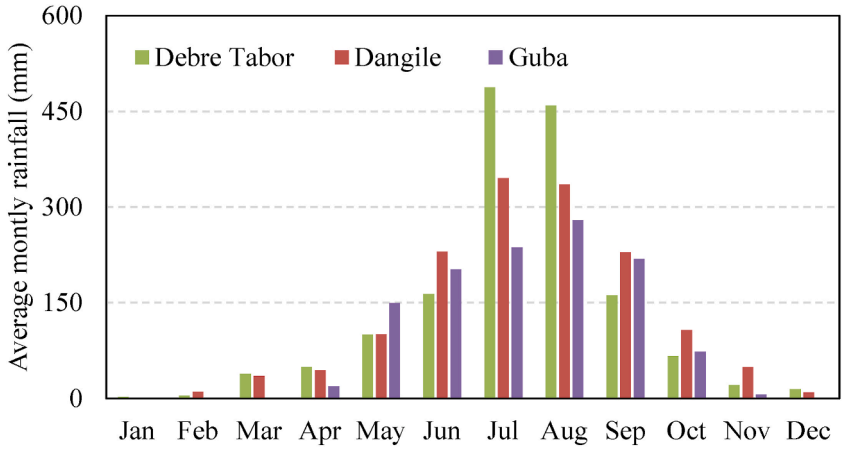

Fig. 3. Average monthly rainfall of three representative stations (i.e., Debre Tabor, Dangila, and Guba) in the Tana-Beles watershed (1990–2020).

Table 2
Classification of the rainfall anomaly index (RAI) and percentage in the Tana-Beles watershed.

RAI Class	RAI range	Percentage
Extremely wet	>2	3.2
Moderately wet	1 to 1.99	16.1
Near-normal	−1 to 0.99	61.4
Moderately dry	−1 to −1.99	16.1
Extremely dry	<-2	3.2

watershed had a moderately wet and moderately dry season, each with RAI between 1 and 2 and RAI between −1 and −2, respectively. For the remaining period (61.4%), the watershed has a near-normal season with RAI between −1 and 1 (Fig. 4).

2.2. Methods

The combined land degradation index mapping was done with the following steps:

(i) Individual land degradation indicators, such as normalized vegetation index (NDVI), salinity index (SI), and albedo, were estimated using GEE on grided data for two periods of ten years span (i.e., 1990 to 2000: 1990s and 2010 to 2020: 2010s).
(ii) The grid values of the individual indicators were standardized to avoid higher emphasis on those variables with a higher variance while identifying the principal component using PCA.
(iii) Anomalies of resampled individual indexes were calculated to determine the percentage contribution of the individual indexes on the combined land degradation index (CLDI).
(iv) The indexes were combined to estimate the CLDI, which was used to examine the extent of land degradation across the Tana-Beles watershed. Fig. 5 presents the framework used to develop a CLDI for the Tana-Beles watershed.
(v) Finally, the highly degraded areas identified using the CLDI were compared with the extremely degraded land digitized from the Google Earth Imagery.

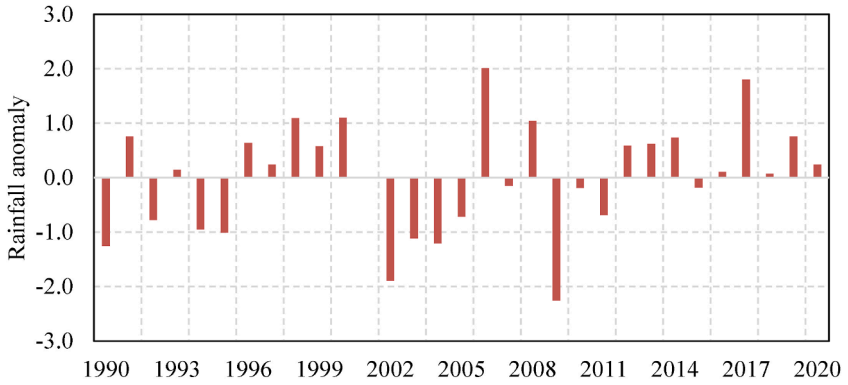

Fig. 4. Time series of annual rainfall anomaly index of the Tana-Beles watershed from 1990 to 2020.

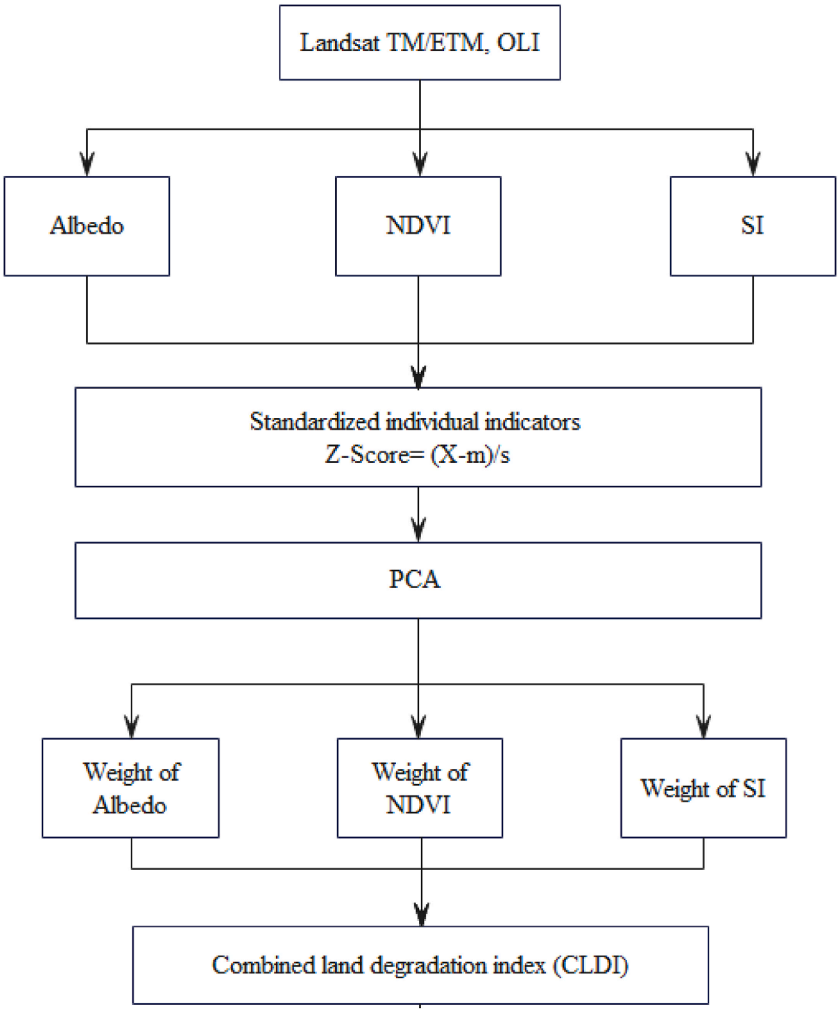

Fig. 5. The general framework developed to identify land degradation in the Tana-Beles watershed. The framework used Albedo, Normalized Vegetation Index (NDVI), and Salinity Index (SI) to develop a combined land degradation index (CLDI).

The individual land degradation index trend was analyzed with a linear regression model with the indexes and time as dependent and independent variables, respectively. The trend analysis was estimated annually using the median values of the indicators to reduce noise and susceptibility to outliers.

The extent of the environmental change within the Tana-Beles watershed was also evaluated by mapping the land use change. The land use change was estimated by applying a supervised classification method for the study periods.

2.2.1. Land degradation proxy indexes

Individual land degradation indicators were estimated using satellite-based input parameters from Landsat TM/ETM and OLI. The individual indexes represent soil exposure (Albedo), vegetation condition (NDVI), and soil health (salinity index SI). For the land degradation assessment, there were 1255 and 1284 Landsat images for the 1990s and 2010s periods, respectively. The methodology to estimate the individual indexes that were used to develop a CLDI is discussed as follows.

2.2.1.1. Albedo. Albedo is estimated as a ratio of the reflected and incident radiation. It is a surface property that controls the amount of energy that is absorbed. Any change in land use condition will be captured by albedo variation. Increased albedo can be used as an indicator of soil degradation, and decreasing albedo may indicate an improvement in land conditions (Jiang et al., 2019). Albedo value can be as high as 0.8 over fresh snow and ice to 0.1 over coniferous forested areas. Albedo values for cropland may range between 0.18 and 0.25, while for bare soils, it may range between 0.05 and 0.5. In this study, albedo is used to represent surface exposure, and it was estimated using spectral bands of Landsat TM/ETM and OLI data using Eqs. (1) and (2) (Liang, 2001; Naegeli et al., 2017).

$$\text{Albedo (TM)} = 0.356\rho_{Blue} + 0.130\rho_{Red} + 0.373\rho_{NIR} + 0.085\rho_{SWIR} + 0.072\rho_{MIR} - 0.0018 \quad \text{(eq-1)}$$

$$\text{Albedo (OLI)} = 0.356\rho_{Blue} + 0.130\rho_{Red} + 0.373\rho_{NIR} + 0.085\rho_{SWIR1} + 0.072\rho_{SWIR2} - 0.0018 \quad \text{(eq-2)}$$

where ρ represents the reflectance of blue, red, near-infrared, and two shortwave-infrared bands of the Landsat TM and OLI imagery.

2.2.1.2. Normalized vegetation index (NDVI). NDVI is estimated by normalizing the difference between the reflectance of the near-infrared and the red channel of the electromagnetic spectrum. NDVI refers to vegetation greenness and above-ground biomass (Berner et al., 2018; Burgan, 1993). NDVI value ranges between −1 and 1, where NDVI < 0 indicates water body or cloud cover and NDVI > 0.6 indicates dense canopy cover. A reduction in vegetation cover is a good indicator of vegetation degradation. A declining trend in climate-adjusted NDVI indicates land degradation, while a rising trend indicates land improvement. The interpretation of NDVI in terms of land degradation or improvement needs to eliminate false alarms that arise from climate variability (Bai et al., 2008a,b).

The NDVI trend analysis was done by applying a linear regression model with NDVI and time as dependent and independent variables, respectively. The trend analysis was estimated using the annual median NDVI values to reduce noise and susceptibility to outliers.

2.2.1.3. Salinization. Soil salinity negatively affects seed germination, crop productivity, soil-water quality, and eventually resulting in the loss of arable lands and soil degradation (John et al., 2005; Kingwell et al., 2008). Excessive salinity changes the soil hydraulic property and reduces water availability to plants. Soil salinization mainly occurred due to inappropriate irrigation practices (i.e., use of poor quality irrigation water, lack of adequate drainage, etc.).

There are multiple procedures to identify salt-affected areas ranging from lab soil samples to remote sensing-based analysis (Metternicht and Zinck, 2003; Rhoades, 1993). For example, this study used remote sensing-based analysis leveraging satellite-retrieved reflectance data of blue and red bands to estimate the salinity index as is presented in equation-3 (Ennaji et al., 2018).

$$\mathbf{SI} = \sqrt{\rho_{\mathbf{Blue}} * \rho_{\mathbf{Red}}} \quad \text{(eq-3)}$$

where SI is the salinity index, $\rho_{\text{Blue,}}$ and ρ_{Red} are the reflectance from the blue and red part of the electromagnetic spectrum, respectively.

2.2.2. Combined land degradation index (CLDI)

The individual land degradation indicators representing vegetation condition, soil health, and surface exposure were combined to develop a CLDI. An objective Principal Component Analysis (PCA) approach was used to quantify the contribution of individual land degradation indexes (i.e., Albedo, NDVI, and SI). PCA is commonly used to reduce the dimensions of a dataset consisting of interrelated indicators or variables (Liang et al., 2009; Partridge and Calvo, 1998). The individual indexes were standardized using the gridded long-term mean and standard deviation data. PCA helps to transfer the individual indexes into a new set of uncorrelated variables to new principal components (PCs). The weights of the PCs are then determined based on the variance explained by each index. The weights are then used to develop the combined land degradation index (Eq-4).

$$\text{CLDI} = w_{\text{albedo}} * \text{Albedo} + w_{\text{NDVI}} * \text{NDVI} + w_{\text{SI}} * \text{SI} \quad \text{eq(4)}$$

where CLDI is the combined land degradation index, Albedo, NDVI, and SI. are the individual indices, while W_{Albedo}, W_{NDVI}, and W_{SI} are their weights.

Finally, the combined land degradation index (CLDI) was normalized with the mean and standardbred deviation and classified into five levels of land degradation (i.e., Extreme, Strong, Moderate, Slight, and no-land degradation).

2.2.3. Validation of the extremely degraded area

The outcomes of the extremely degraded area using the CLDI were compared with the extremely degraded area digitized from the Google Earth Imagery. According to Young (1994), an extremely degraded area is characterized as regions that are irreclaimable and beyond restoration, with their original biotic functions fully destroyed. To identify the irreclaimable and beyond restoration area, land degradation was digitized annually from 2010 to 2020 using the Google Earth Imagery platform, and the intersecting area was designated as irreclaimable. Finally, both datasets were compared to assess the performance of the CLDI indicator.

2.2.4. Evaluation of environmental changes across tana-Beles watershed

Environmental changes across the study area were evaluated by assessing the land use change. The land use change was studied using a supervised land use classification method for the 1990s and 2010s periods. Training data for land use classification were collected from Google Earth, including forest, agricultural land, bare land, wetland, urban, and bushland.

3. Results and discussion

3.1. Land degradation condition

The individual land degradation indicators were estimated using eq-1, 2, and 3 over two mosaic Landsat images across the Tana-Beles watershed at a spatial resolution of 30 m. For the first study period, 1990 to 2000, there were 1255 images, and for the second period (2010–2020), there were 1284 images. The soil surface exposure was evaluated using Eqs. (1) and (2) using Landsat images for the 1990s and 2010s periods (Fig. 6a and b). The analysis indicated that the albedo of the Tana-Beles watershed increased by 97% during the 2010s compared to the 1990s (Fig. 6b). At the watershed level, in Beles, the albedo increased by 101%, and in Tana increased by 94% in the 2010s compared to the 1990s. The histogram of the change in albedo was constructed (albedo of the 2010s mi-

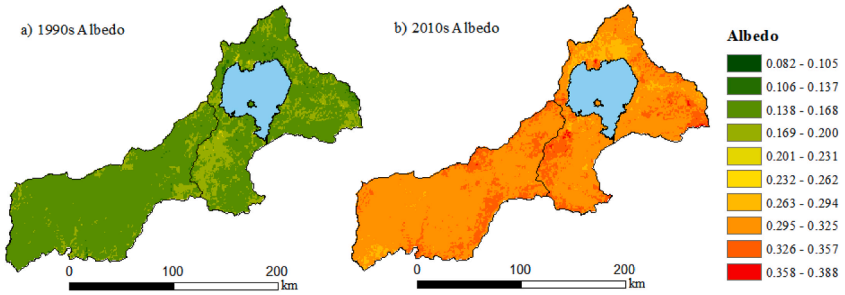

Fig. 6. The average Albedo of the 1990s and 2010s of the study area. (a) 199s Albedo and (b) 2010s Albedo.

nus albedo of 1990s), and the histogram indicated that during the study period, albedo increased all over the watershed (Fig. 7). The change in albedo will affect evapotranspiration since albedo is a primary factor partitioning sensible and latent heat fluxes. The increased albedo will have a warming effect across the environment and subsequently altering the hydrological cycle (Qian et al., 2011).

The NDVI analysis indicated that in the 1990s, the average NDVI was approximately 0.305, which decreased significantly by 23%, reaching 0.232 in the 2010s (Fig. 8). Almost 98.5% of the study area's vegetation condition deteriorated; see the histogram of the change in NDVI calculated as the difference between the average NDVI of the 2010s and 1990s (Fig. 9). At the watershed level, vegetation conditions deteriorated at 25.7% and 22.6% in Beles and Tana watersheds, respectively. The annual NDVI trend analysis also indicated a decreasing trend in the 1990s and 2010s. The deforestation in the watershed is mainly driven by agricultural land expansion and uncontrolled wildfires (Desta, 2014).

The SI analysis indicated that salinity had increased significantly from the 1990s (Fig. 10). The average salinity index across the study site in the 1990s was ~0.113 and increased to ~0.205 in the 2010s (82% increase). In the 2010s, the salinity index in the Lake Tana watershed is higher, especially in the east and west of Lake Tana. The histogram of the change in the salinity index across the Tana-Beles watershed (salinity of the 2010s minus 1990s) is shown in Fig. 11. It shows that salinity has increased all over the watershed. However, according to Moreira et al. (2015) and Asfaw et al. (2018), the soil salinity in the Tana-Beles watershed can be considered as non-saline since the salinity index is less than 0.4 or 2 ECe.

3.2. Combined land degradation in Tana-Beles watershed

The correlation of the three major forms of land degradation indicators was evaluated with a Pearson's correlation coefficient (Table 3). The result indicated that for both study periods (the 1990s and 2010s), NDVI and salinity index indicated a strong negative

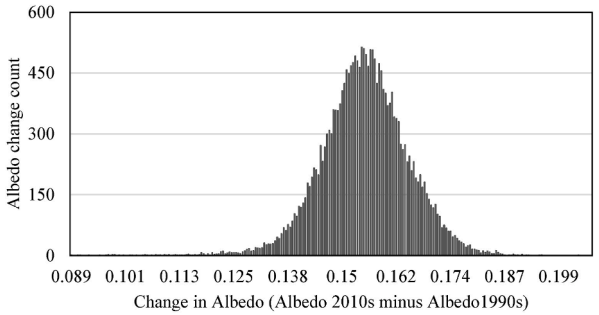

Fig. 7. The histogram of the change in albedo across the Tana-Beles watershed (2010s albedo minus 1990s albedo).

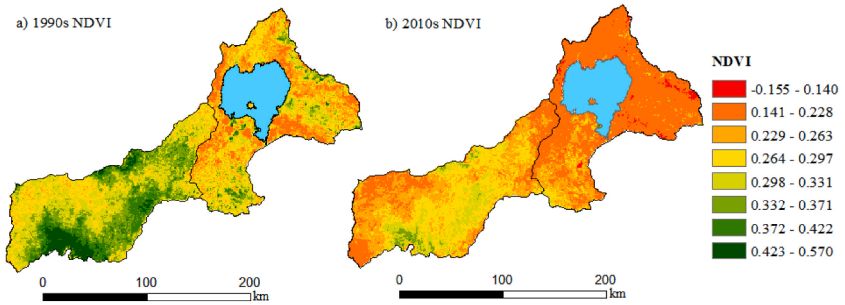

Fig. 8. The average NDVI of the Tana-Beles watershed of the 1990s and 2010s. (a) 1990s NDVI and (b) 2010s NDVI.

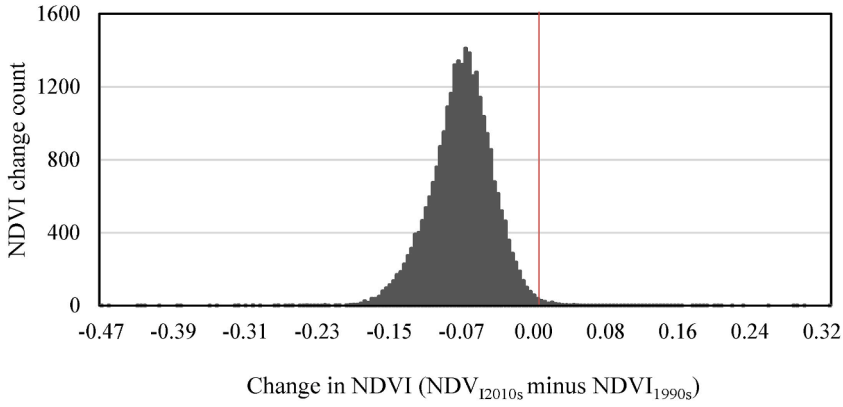

Fig. 9. The histogram of the change in NDVI across the Tana-Beles watershed (2010s NDVI minus 1990s NDVI).

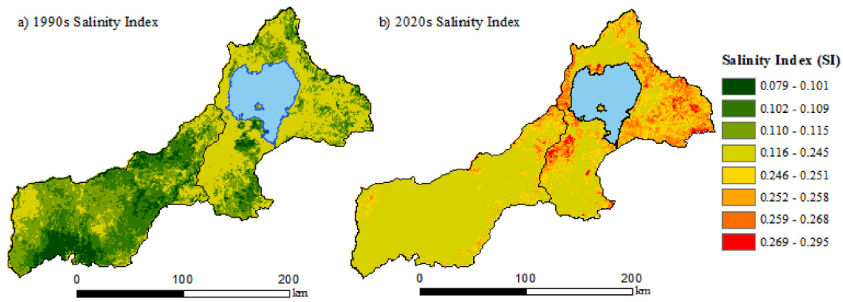

Fig. 10. Lake-Tana watershed average soil salinity index of the 1990s and 2010s. (a) 1990s salintiy index and (b) 2010s salintiy index.

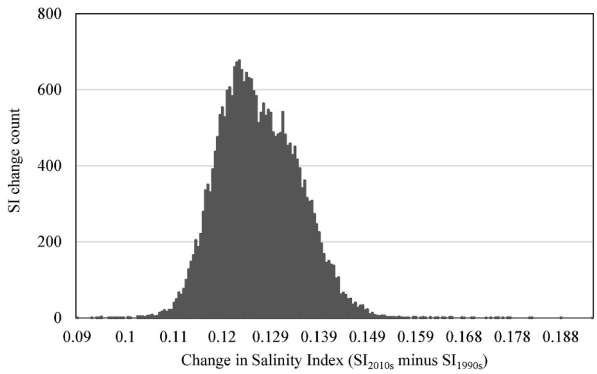

Fig. 11. The histogram of the change in soil salinity index in the Tana-Beles watershed (2010s soil salinity index minus 1990s soil salinity index).

Table 3
Correlation between individual land degradation indicators for the 1990s and 2010s.

Correlation (1990s)	NDVI	Albedo	Salinity index
NDVI	1.00	−0.09	−0.76
Albedo		1.00	0.66
Salinity index			1.00
Correlation (2010s)	**NDVI**	**Albedo**	**Salinity index**
NDVI	1.00	0.23	−0.71
Albedo		1.00	0.48
Salinity index			1.00

linear relationship, demonstrating a clear reduction in vegetation cover with increasing salinity. Previous studies also revealed a negative linear relationship between NDVI and salinity (Al-Khakani and Sa'ad, 2019; Aldakheel, 2011). The salinity index exhibited a positive linear correlation with the Albedo in both the 1990s and 2010s. However, during the 2010s, the correlation was comparatively weaker than in the 1990s, primarily due to an uneven increase in their respective indexes. Particularly, the albedo saw a significant 101% surge caused by extensive deforestation in the watershed, while the salinity increased by 82%. These divergent albedo and salinity index trends notably diminished their correlation during the 2020s. The analysis did not show a linear association between NDVI (vegetation condition) and albedo (soil exposure) across the study site. This could be due to the fact that in the study site, albedo is more related to soil moisture and precipitation (Samain et al., 2008).

The PCA was used to combine the relevant indicators to develop a combined land degradation indicator. The weights of individual indexes of the 1990s were 96%, 3.4%, and 0.6% for NDVI, Albedo, and Salinity index, respectively. For the 2010s, the weights of the individual indicators were 91%, 8.5%, and 0.5% for NDVI, Albedo, and Salinity index.

The combined land degradation index was reclassified into four classes applying the natural breaks classification method, also known as Jenks' optimization (Chen et al., 2013; Naiqiang and Guiyang, 2020). This approach relies on identifying natural groupings in the data, where similar values were grouped together while maximizing the distinctions between classes and minimizing the variability within each class. This method has been used to reclassification multiple indicators, including land degradation index, soil erosion, and albedo (Achour et al., 2021; Arabameri et al., 2018; Hashem Geloogerdi et al., 2021; Jaafari et al., 2022). The reclassified combined land degradation of the 2010s indicated that a fraction of the study area, ~2% is extremely degraded, while 18%, 43%, and 27% are strongly, moderately, and slightly degraded, respectively (Fig. 12). The remaining area (~10%) is not degraded. Almost all of the extremely degraded land is located in Lake Tana, occupying 4.3% of the watershed. Interestingly, nearly 93% of the non-degraded land is located in the Beles watershed.

The CLDI analysis revealed the presence of 23 highly degraded areas within the Lake Tana watershed, varying in size from 1 km^2 to 43 km^2. The largest among them is situated to the east of Lake Tana, near Guna Mount. By digitizing the extremely degraded areas on Google Earth Imagery, a total of 18 degraded areas were identified and distributed across the watershed. A comparison between the results obtained from the CLDI and the digitization process demonstrated a 74.5% match, indicating an acceptable performance of the CLDI in identifying degraded areas.

3.3. Effect of land degradation in the Tana-Beles watershed

A Landsat image was processed to map the major land use groups by applying a supervised classification (Fig. 13). The accuracy of the land use classification was assessed to determine how well the land use classification was completed by applying a confusion matrix. The accuracy assessment indicated an acceptable performance with 95% and 96% for the 1990s and 2010s, respectively. The 1990s land use classification indicated that approximately half of the watershed was coved with bushland, followed by cropland (21%), bareland (11%), waterbody (11%), and forest (7%), while the remaining part of the watershed was covered with wetland and settlement (Fig. 13a). In the 2010s, the fraction of bushland reduced significantly, covering only 37% of the watershed; most of the

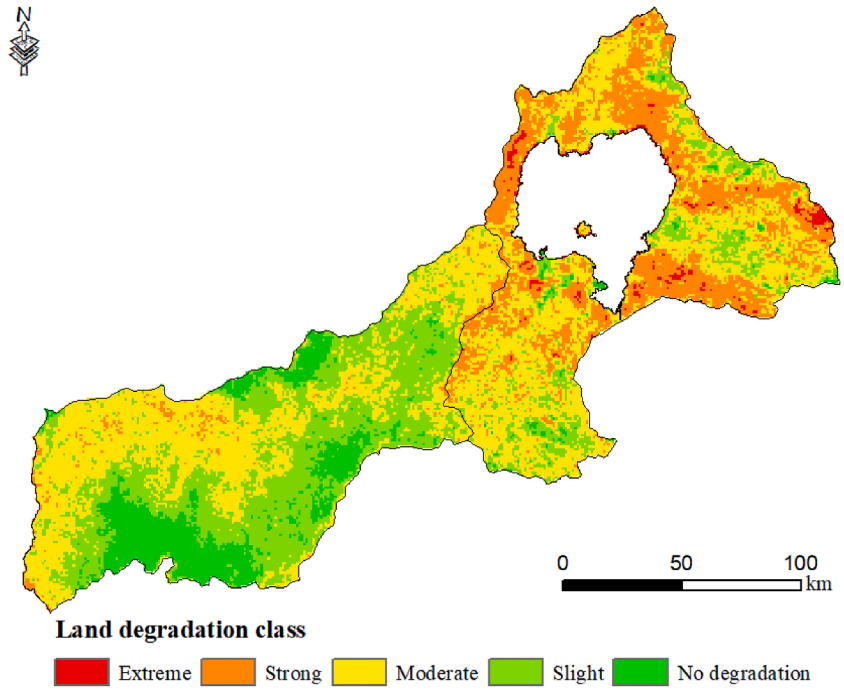

Fig. 12. The spatial extent of the land degradation class for the 2010s.

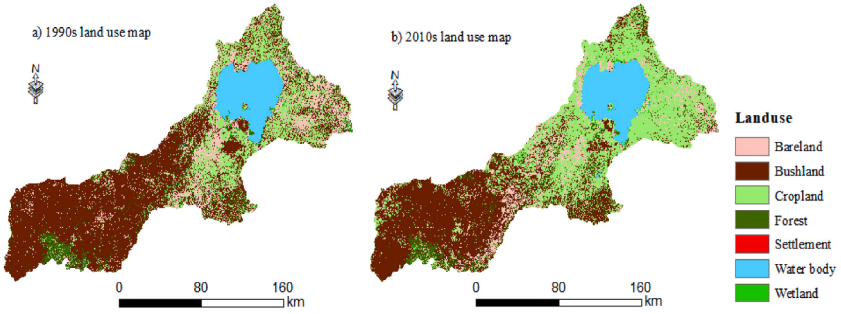

Fig. 13. Land use map of Tana-Beles watersehd.

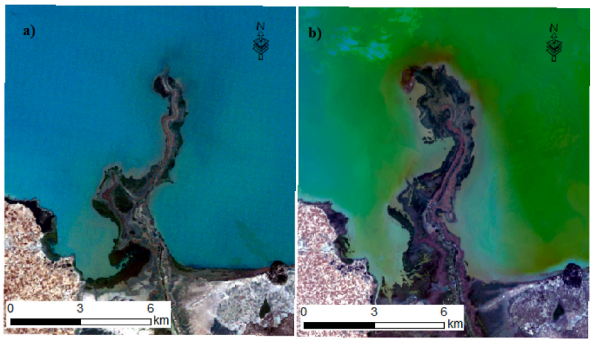

Fig. 14. The size of Gilgel Abay River mouth delta. (a) 1990s Gilgel Abay River mouth delta, and (b) 2010s Gilgel Abay River mouth delta.

bushland, especially in the Beles watershed, was converted to cropland. The agricultural land has increased significantly, reaching 37% of the watershed. Also, some fractions of the bareland and forest land in the 1990s were converted to agricultural land (Fig. 13b). The land use changes led to significant changes in the surface albedo.

A closer look into the river mouth delta of the major tributaries of Lake Tana indicated a considerable expansion due to sediment deposition. The size of the river mouth delta compared to similar lake levels indicated a 49% increase in size in the 2010s (i.e., from 14.6 km^2 to 21.8 km^2) compared to the 1990s (Fig. 14). Due to rapid land use conversion in the head watershed, the surface runoff brings sediment along with nutrients from the fertilizer applied in the agricultural area has caused the eutrophication of the lake. Making the lake a fertile ground for invasive aquatic crops. A recent study by (Dersseh et al., 2019; Enyew et al., 2020; Tewabe, 2015) indicated that the invasive aquatic crop, water hyacinth, is growing exponentially in the northeast corridor of the lake.

4. Conclusions

This study examined the spatial extent of land degradation in the Upper Blue Nile Basin by combining indicators representing soil exposure (Albedo), vegetation condition (NDVI), and soil health (salinity index SI). The individual land degradation indicators were estimated for the 1990s and 2010s. The indicators were combined with a Principal Component Analysis (PCA) to develop a Combined Land Degradation Index (CLDI). Moreover, the study also evaluated the extent of land degradation by applying a supervised land use classification. The result of the analysis indicated that land degradation is the major issue in the Tana-Beles watershed, where the soil exposure and soil salinity decreased by 97 and 82% at the same time the vegetation condition deteriorated compared to the 1990s. In the 2010s, ~63% of Tana-Beles is estimated to be moderate to extremely degraded. The land use change analysis also indicated a significant agricultural expansion at the cost of bushland and bareland. This study could provide valuable insight to put in place effective best management practices across the study site to offer the opportunity to reverse and stabilize the landscape.

Author statement

Abeyou W. Worqlul: Conceptualization, Methodology, Investigation, Data Curation, Writing-original draft, and Validation. **Mira Haddad**: Data curation, Writing- Reviewing and Editing. **Sintayehu Alemayehu**: Writing- Reviewing and Editing. **Ajit Govind**: Writing- Reviewing and Editing.

Declaration of competing interest

The authors declare that they have no known competing financial interests or personal relationships that could have appeared to influence the work reported in this paper.

Data availability

Data will be made available on request.

Acknowledgments:

We acknowledge the funding from the Belgium CGIAR Fund Addressing SDG15 in the Sahel by Building Pathways for Transforming Food and Land Systems in a Climate Crisis. This was made available through the WP1 of CGIAR ClimBeR Initiative: Building Systemic Resilience against Climate Variability and Extremes. We would also like to express our gratitude for the support provided by the Livestock, Climate, and System Resilience (LCSR) of the OneCGIAR.

References

Al-Khakani, E.T., Sa'ad, R.Y., 2019. An assessment of soil salinity and vegetation cover changes for a part of An-Najaf governorate using remote sensing data. J. Phys. Conf. 1234, 012023.
Achour, Y., Saidani, Z., Touati, R., Pham, Q.B., Pal, S.C., Mustafa, F., Balik Sanli, F., 2021. Assessing landslide susceptibility using a machine learning-based approach to achieving land degradation neutrality. Environ. Earth Sci. 80, 1–20.
Aldakheel, Y.Y., 2011. Assessing NDVI spatial pattern as related to irrigation and soil salinity management in Al-Hassa Oasis, Saudi Arabia. J. Indian Soc. Remote Sens. 39, 171–180.
Arabameri, A., Rezaei, K., Pourghasemi, H.R., Lee, S., Yamani, M., 2018. GIS-based gully erosion susceptibility mapping: a comparison among three data-driven models and AHP knowledge-based technique. Environ. Earth Sci. 77, 1–22.
Asfaw, E., Suryabhagavan, K., Argaw, M., 2018. Soil salinity modeling and mapping using remote sensing and GIS: the case of Wonji sugar cane irrigation farm, Ethiopia. J. Saudi Soc. Agric. Sci. 17 (3), 250–258.
Bai, Z., Dent, D.L., Olsson, L., Schaepman, M.E., 2008a. Global Assessment of Land Degradation and Improvement: 1. identification by remote sensing.
Bai, Z.G., Dent, D.L., Olsson, L., Schaepman, M.E., 2008b. Proxy global assessment of land degradation. Soil Use Manag. 24 (3), 223–234.
Bayissa, Y.A., Tadesse, T., Svoboda, M., Wardlow, B., Poulsen, C., Swigart, J., Van Andel, S.J., 2019. Developing a satellite-based combined drought indicator to monitor agricultural drought: a case study for Ethiopia. GIScience Remote Sens. 56 (5), 718–748.
Berner, L.T., Jantz, P., Tape, K.D., Goetz, S.J., 2018. Tundra plant above-ground biomass and shrub dominance mapped across the North Slope of Alaska. Environ. Res. Lett. 13 (3), 035002.
Burgan, R.E., 1993. Monitoring Vegetation Greenness with Satellite Data, vol. 297. US Department of Agriculture, Forest Service, Intermountain Research Station.
Chen, J., Yang, S., Li, H., Zhang, B., Lv, J., 2013. Research on geographical environment unit division based on the method of natural breaks (Jenks). Int. Arch. Photogram. Rem. Sens. Spatial Inf. Sci. 40, 47–50.
Chen, S., Rao, P., 2008. Land degradation monitoring using multi-temporal Landsat TM/ETM data in a transition zone between grassland and cropland of northeast China. Int. J. Rem. Sens. 29 (7), 2055–2073.
Chikhaoui, M., Bonn, F., Bokoye, A.I., Merzouk, A., 2005. A spectral index for land degradation mapping using ASTER data: application to a semi-arid Mediterranean catchment. Int. J. Appl. Earth Obs. Geoinf. 7 (2), 140–153.
Dersseh, M.G., Melesse, A.M., Tilahun, S.A., Abate, M., Dagnew, D.C., 2019. Water hyacinth: review of its impacts on hydrology and ecosystem services—lessons for management of Lake Tana. Extreme Hydrol. Clim. Variab. 237–251.
Desta, S.B., 2014. Deforestation and a strategy for rehabilitation in beles sub basin, Ethiopia. J. Econ. Sustain. Dev. 5 (15).
Easdale, M.H., Bruzzone, O., Mapfumo, P., Tittonell, P., 2018. Phases or regimes? R evisiting NDVI trends as proxies for land degradation. Land Degrad. Dev. 29 (3), 433–445.
Eckert, S., Hüsler, F., Liniger, H., Hodel, E., 2015. Trend analysis of MODIS NDVI time series for detecting land degradation and regeneration in Mongolia. J. Arid Environ. 113, 16–28.
Elaalem, M., Comber, A., Fisher, P., 2011. A comparison of fuzzy AHP and ideal point methods for evaluating land suitability. Trans. GIS 15 (3), 329–346.
Ennaji, W., Barakat, A., Karaoui, I., El Baghdadi, M., Arioua, A., 2018. Remote sensing approach to assess salt-affected soils in the north-east part of Tadla plain, Morocco. Geol., Ecol., Landscapes 2 (1), 22–28.
Enyew, B.G., Assefa, W.W., Gezie, A., 2020. Socioeconomic effects of water hyacinth (echhornia Crassipes) in Lake Tana, north western Ethiopia. PLoS One 15 (9), e0237668.
Farr, T.G., Rosen, P.A., Caro, E., Crippen, R., Duren, R., Hensley, S., Roth, L., 2007. The shuttle radar topography mission. Rev. Geophys. 45 (2).
Ferrer-i-Carbonell, A., Gowdy, J.M., 2007. Environmental degradation and happiness. Ecol. Econ. 60 (3), 509–516.
Funk, C., Peterson, P., Landsfeld, M., Pedreros, D., Verdin, J., Shukla, S., Hoell, A., 2015. The climate hazards infrared precipitation with stations—a new environmental record for monitoring extremes. Sci. Data 2 (1), 1–21.
Gebreselassie, S., Kirui, O.K., Mirzabaev, A., 2016. Economics of land degradation and improvement in Ethiopia. In: Economics of Land Degradation and Improvement–A Global Assessment for Sustainable Development. Springer, Cham, pp. 401–430.
Gibbs, H., Salmon, J.M., 2015. Mapping the world's degraded lands. Appl. Geogr. 57, 12–21.
Gorelick, N., Hancher, M., Dixon, M., Ilyushchenko, S., Thau, D., Moore, R., 2017. Google Earth Engine: planetary-scale geospatial analysis for everyone. Remote Sens. Environ. 202, 18–27.
Haberl, H., Erb, K.H., Krausmann, F., Gaube, V., Bondeau, A., Plutzar, C., Fischer-Kowalski, M., 2007. Quantifying and mapping the human appropriation of net primary production in earth's terrestrial ecosystems. Proc. Natl. Acad. Sci. USA 104 (31), 12942–12947.
Hashem Geloogerdi, S., Vali, A., Sharifi, M.R., 2021. Application of TGSI-Albedo feature space model in assessing of desertification status in the center of Khuzestan province. Desert Manag. 9 (3), 49–66.
Higginbottom, T.P., Symeonakis, E., 2014. Assessing land degradation and desertification using vegetation index data: Current frameworks and future directions. Rem. Sens. 6 (10), 9552–9575.
Hoang, H.T., Truong, Q.H., Nguyen, A.T., Hens, L., 2018. Multicriteria evaluation of tourism potential in the central highlands of vietnam: combining geographic information system (GIS), analytic hierarchy process (AHP) and principal component analysis (PCA). Sustainability 10 (9), 3097.
Ibrahim, Y.Z., Balzter, H., Kaduk, J., Tucker, C.J., 2015. Land degradation assessment using residual trend analysis of GIMMS NDVI3g, soil moisture and rainfall in Sub-Saharan West Africa from 1982 to 2012. Rem. Sens. 7 (5), 5471–5494.
Jaafari, A., Janizadeh, S., Abdo, H.G., Mafi-Gholami, D., Adeli, B., 2022. Understanding land degradation induced by gully erosion from the perspective of different geoenvironmental factors. J. Environ. Manag. 315, 115181.
Jiang, L., Jiapaer, G., Bao, A., Li, Y., Guo, H., Zheng, G., De Maeyer, P., 2019. Assessing land degradation and quantifying its drivers in the Amudarya River delta. Ecol. Indicat. 107, 105595.
John, M., Pannell, D., Kingwell, R., 2005. Climate change and the economics of farm management in the face of land degradation: dryland salinity in Western Australia. Can. J. Agric. Econ./Rev. can. d'agroecon. 53 (4), 443–459.
Katz, R.W., Glantz, M.H., 1986. Anatomy of a rainfall index. Mon. Weather Rev. 114 (4), 764–771.
Kebede, Y.S., Endalamaw, N.T., Sinshaw, B.G., Atinkut, H.B., 2021. Modeling soil erosion using RUSLE and GIS at watershed level in the upper beles, Ethiopia. Environ. Challenges 2, 100009.
Kingwell, R., John, M., Robertson, M., 2008. A review of a community-based approach to combating land degradation: dryland salinity management in Australia. Environ. Dev. Sustain. 10 (6), 899–912.

Kong, G., Jiang, L., Yin, X., Wang, T., Xu, D.-L., Yang, J.-B., Hu, Y., 2018. Combining principal component analysis and the evidential reasoning approach for healthcare quality assessment. Ann. Oper. Res. 271 (2), 679–699.
Le, Q.B., Nkonya, E., Mirzabaev, A., 2016. Biomass productivity-based mapping of global land degradation hotspots. Econ. Land Degrad. Improve.–Global Assess. Sustain. Dev. 55.
Liang, L., Li, Y., Li, S., 2009. Increasing the discriminatory power of DEA in the presence of the undesirable outputs and large dimensionality of data sets with PCA. Expert Syst. Appl. 36 (3), 5895–5899.
Liang, S., 2001. Narrowband to broadband conversions of land surface albedo I: algorithms. Remote Sens. Environ. 76 (2), 213–238.
Liu, F., Chen, Y., Lu, H., Shao, H., 2017. Albedo indicating land degradation around the Badain Jaran Desert for better land resources utilization. Sci. Total Environ. 578, 67–73.
Mallick, S.K., Rudra, S., 2021. Analysis of groundwater potentiality zones of Siliguri urban agglomeration using GIS-based fuzzy-AHP approach. In: Groundwater and Society. Springer, pp. 141–160.
Manandhar, R., Odeh, I.O., 2014. Interrelationships of land use/cover change and topography with soil acidity and salinity as indicators of land degradation. Land 3 (1), 282–299.
Mariano, D.A., dos Santos, C.A., Wardlow, B.D., Anderson, M.C., Schiltmeyer, A.V., Tadesse, T., Svoboda, M.D., 2018. Use of remote sensing indicators to assess effects of drought and human-induced land degradation on ecosystem health in Northeastern Brazil. Remote Sens. Environ. 213, 129–143.
Metternicht, G.I., Zinck, J., 2003. Remote sensing of soil salinity: potentials and constraints. Remote Sens. Environ. 85 (1), 1–20.
Moore, R., Hansen, M., 2011. Google Earth Engine: a new cloud-computing platform for global-scale earth observation data and analysis. AGU Fall Meeting Abstracts.
Moreira, L.C.J., Teixeira, A.d.S., Galvão, L.S., 2015. Potential of multispectral and hyperspectral data to detect saline-exposed soils in Brazil. GIScience Remote Sens. 52 (4), 416–436.
Naegeli, K., Damm, A., Huss, M., Wulf, H., Schaepman, M., Hoelzle, M., 2017. Cross-comparison of albedo products for glacier surfaces derived from airborne and satellite (Sentinel-2 and Landsat 8) optical data. Rem. Sens. 9 (2), 110.
Naiqiang, L., Guiyang, X., 2020. Grid analysis of land use based on natural breaks (jenks) classification. Bull. Surv. Mapp. (4), 106.
Olsson, L., Barbosa, H., Bhadwal, S., Cowie, A., Delusca, K., Flores-Renteria, D., Li, D., 2019. Land Degradation. Climate Change and Land: an IPCC Special Report on Climate Change, Desertification, Land Degradation, Sustainable Land Management, Food Security, and Greenhouse Gas Fluxes in Terrestrial Ecosystems. pp. 345–436.
Partridge, M., Calvo, R.A., 1998. Fast dimensionality reduction and simple PCA. Intell. Data Anal. 2 (3), 203–214.
Qian, Y., Flanner, M., Leung, L., Wang, W., 2011. Sensitivity studies on the impacts of Tibetan Plateau snowpack pollution on the Asian hydrological cycle and monsoon climate. Atmos. Chem. Phys. 11 (5), 1929–1948.
Rhoades, J., 1993. Electrical conductivity methods for measuring and mapping soil salinity. Adv. Agron. 49, 201–251.
Samain, O., Kergoat, L., Hiernaux, P., Guichard, F., Mougin, E., Timouk, F., Lavenu, F., 2008. Analysis of the in situ and MODIS albedo variability at multiple timescales in the Sahel. J. Geophys. Res. Atmos. 113 (D14).
Surur, A., 2010. Simulated Impact of Land Use Dynamics on Hydrology during a 20-Year-Period of Beles Basin in Ethiopia.
Taddese, G., 2001. Land degradation: a challenge to Ethiopia. Environ. Manag. 27 (6), 815–824.
Temesgen, G., Amare, B., Silassie, H., 2014. Land degradation in Ethiopia: causes, impacts and rehabilitation techniques. J. Environ. Earth Sci. 4 (9), 98–104.
Tewabe, D., 2015. Preliminary survey of water hyacinth in Lake Tana, Ethiopia. Global J. Allergy 1 (1), 13–18.
UNCCD, 2002. Recommendations and Conclusions of the African Regional Conference Preparatory to the First Session of the Committee for the Review of the Implementation of the United Nations Convention to Combat Desertification (UNCCD–CRIC1).
Wessels, K.J., Prince, S., Frost, P., Van Zyl, D., 2004. Assessing the effects of human-induced land degradation in the former homelands of northern South Africa with a 1 km AVHRR NDVI time-series. Remote Sens. Environ. 91 (1), 47–67.
Worqlul, A.W., Dile, Y.T., Bezabih, M., Adie, A., Srinivasan, R., Lefore, N., Clarke, N., 2022. Identification of suitable areas for fodder production in Ethiopia. Catena 213, 106154.
Worqlul, A.W., Dile, Y.T., Schmitter, P., Jeong, J., Meki, M.N., Gerik, T.J., Clarke, N., 2019. Water resource assessment, gaps, and constraints of vegetable production in Robit and Dangishta watersheds, Upper Blue Nile Basin, Ethiopia. Agric. Water Manag. 226, 105767.
Young, A., 1994. Land Degradation in South Asia: its Severity, Causes, and Effects upon the People.–World Soil Resources Report 78.
Yu, T., Jiapaer, G., Bao, A., Zheng, G., Jiang, L., Yuan, Y., Huang, X., 2021. Using synthetic remote sensing indicators to monitor the land degradation in a salinized area. Rem. Sens. 13 (15), 2851.